Journal of Materials Chemistry A

Accepted Manuscript

ROYAL SOCIETY OF CHEMISTRY

www.rsc.org/materialsA

Oxygen Non-stoichiometry, Conductivity and Gas Sensor Response of SnO_2 Pellets

Ibtessam A Alagdal and Anthony R West

University of Sheffield
Dept of Material Science and Engineering
Mappin Street
Sheffield S1 3JD
United Kingdom

ABSTRACT

SnO_2 pellets lose a very small amount of oxygen at high temperatures to give, for instance, the stoichiometry $SnO_{1.9989(1)}$ at 1200 °C in air. The oxygen deficiency, δ can be preserved at ambient temperature in quenched samples. The level of conductivity, which is n-type, depends on oxygen content, 2-δ and varies by several orders of magnitude; activation energies cover the range 1.1 eV for slow-cooled, fully oxidised samples to 0.52 eV for samples quenched from 1200 °C. Quenched samples can be readily and reversibly reoxidised and reduced at temperatures as low as 700 °C; at lower temperatures, down to ~ 350 °C, oxidation and reduction is mainly confined to sample surfaces on short timescales but, nevertheless, is sufficient for the conductivity to change by 1 to 2 orders of magnitude. Quenched, oxygen-deficient samples are also moisture-sensitive whereas fully oxidised samples are not. SnO_2 shows similar sensitivity to both CO_2 and N_2, which is attributed to loss of O_2 from the sample surface.

INTRODUCTION

Tin oxide, SnO_2 , both pure and doped, has many applications as a functional material which can be grouped into three main areas, as a (i) a solid state gas sensor, (ii) an oxidation catalyst and (iii) a transparent conducting oxide, TCO[1–3] . The first two applications are surface-driven whereas TCO's are used for their bulk properties.

For surface-driven applications, sample fabrication is important and SnO_2 has been prepared in many forms and by various methods including, as examples, porous materials, [4] sol-gel derived nano particles[5], inductively-coupled plasma nanorods [6], *dc* magnetron-deposited thin films together with Pt, Pd catalyst particles on the surface[7], hydrothermally-prepared nanoplatelets[8] and electrochemically-anodised films[9]. The nature and mechanism of gas-surface interactions are key to the use of

SnO_2 as both a catalyst in industrial oxidative dehydrogenation and as a sensor of reducing gases. Nevertheless, the mechanistic details are still a matter of debate, especially the effects of O_2 and H_2O on the sensor conductivity.

There are numerous comments in the literature [10-12] about the possibility of oxygen non-stoichiometry, with the formula $SnO_{2-\delta}$, but the value(s) of δ and its possible dependence on sample processing conditions has not been quantified. It is stated that a key method to introduce oxygen vacancies into SnO_2 is to use a divalent tin compound, $SnCl_2.2H_2O$, as the precursor in hydrothermal synthesis [10], with evidence for oxygen vacancies obtained by both X-ray photoelectron spectroscopy, XPS and electron spin resonance, ESR, spectroscopy. The electrical conductivity of $SnO_{2-\delta}$ is n-type whereas that of the oxygen-rich divalent oxide, $SnO_{1+\delta}$ is p-type[11]. Instances of p-type conductivity in SnO_2 films have been attributed to the presence of SnO-like regions within films that were shown to be inhomogeneous[11] and contained both SnO_2- and SnO-like regions.

Impedance spectroscopy, IS, has been used to characterise SnO_2 films prepared by two methods, rf magnetron sputtering of thin films and doctor blade deposition of thick films followed by heating in air at 500 °C for 2 hrs [12]. Using IS, the sensitivity of the films to N_2/O_2 at 150 and 200 °C was studied; film resistance increased in O_2 and decreased in N_2, consistent with n-type behaviour.

Several studies of the effect of H_2O adsorption on SnO_2 have been reported [13-20]. Different mechanisms of SnO_2 - H_2O interaction have been proposed, depending on the structure of the SnO_2 surface and explanations given for the observed changes in conductivity. For instance, it was suggested that absorption of H_2O leads to band-bending within the SnO_2 electronic structure and an associated increase in conductivity [13].

The interaction of SnO_2 surfaces with O_2, H_2O and H_2 was investigated by temperature programmed desorption, TPD, chromatography [14]. Evidence was found for four kinds of oxygen species which desorbed at 80 °C (O_2), 150 °C (O_2^-), 560 °C (O^- or O^{2-}) and > 600 °C (lattice O^{2-}). O_2^-, O^- and O^{2-} were described as *depletive adsorbates* since on desorption, electrons were released (together with gaseous O_2) leading to an increase in conductivity. Two kinds of adsorbed H_2O species were identified similarly by TPD, at 100 °C (molecular H_2O) and 400 °C (OH groups). Release of OH groups, but not H_2O molecules, was accompanied by a decrease in conductivity although the mechanism responsible for the change in conductivity was not clear[14].

The main purposes of the present work were: first, to establish whether SnO_2 showed a temperature-dependent variation in oxygen content of the kind shown by rutile, TiO_2 which has the same crystal structure as SnO_2 [21]; second, to determine the conductivity of SnO_2 pellets as a function of any oxygen non-stoichiometry and sample processing conditions; third, to establish the effect of possible oxygen non-stoichiometry on sensitivity to O_2, N_2, CO_2 and H_2O.

EXPERIMENTAL

High purity SnO_2 (99.9 % Sigma Aldrich) was ground to a fine powder with an agate mortar and pestle, pressed into pellets of 20 mm diameter at 0.6 tonnes, placed on sacrificial SnO_2 powder in a Pt crucible and fired at 1300 ^oC for 8 hrs in air. The sintered pellets were then given subsequent heat treatments, either at temperatures in the range 800 to 1200 ^oC in air for 2 hours followed by quenching to room temperature (by removing from the furnace and allowing to cool in air, typically over a period of 1-2 mins), or at 900 ^oC in O_2 for 2 hrs followed by slow cool in O_2 to room temperature (by switching off the furnace). Typical pellet densities were 50-62 % with a porous microstructure consisting of interconnected grains of size ~ 0.5 – 2.5 μm, Fig 1.

Pellets for IS measurements were coated with Pt paste on opposite faces which was dried and hardened at 900 ^oC for 1 hr to form electrodes. These were attached to Pt leads in a conductivity jig, which was placed inside a horizontal tube furnace through which different gases could be passed, allowed to equilibrate, typically for 10 – 30 mins and then IS data recorded. In general, Pt electrodes were fabricated before the final heat treatments to avoid possible unwanted oxidation/reduction prior to the IS measurements. Measurements were made isothermally in the temperature range 200 to 700 ^oC and over the frequency range 10 Hz to 1 MHz using Hewlett Packard 4192A instrumentation. Impedance data were corrected for overall pellet geometry and are reported in units of resistance: ohm cm and capacitance : F cm^{-1}; data were not corrected for the geometry of regions such as grain boundaries since this was not known accurately.

In order to measure changes in sample mass as a function of temperature, thermogravimetry, TG, could not be used as the mass changes (a few micrograms) were too small to be detected reliably with available TG instrumentation. Instead, the mass of a pellet of approximately 2 g was measured on a microbalance after a range of heat treatments. The same pellet was placed in a Pt boat, heated isothermally for 1 hr over the range 25 – 1200 ^oC, cooled rapidly to room temperature and its mass recorded before returning to the furnace. Data were obtained stepwise on both heating and cooling.

RESULTS and DISCUSSION

All pellets used for the results reported here were sintered initially at 1300^{o}C for 8 hrs in air and then given a range of follow-on heat treatments. X-ray powder diffraction, XRD, on crushed pellet fragments confirmed that the samples were phase-pure SnO_2 with the rutile structure after various heat treatments. Detection of secondary phases by XRD is typically at the 1-2% level and the technique is therefore insensitive to, for instance, any small changes in surface structure or composition.

For weight change studies, a pellet of mass ~ 2 g was given a second heating at 900 ^{o}C in O_2 for 2 h, slow-cooled to room temperature and then reheated in air isothermally at different temperatures, quenched to room temperature and its mass recorded. Data are summarised in Fig 2 for stepwise heating and cooling of the same sample. In order to assign values of δ to the oxygen contents, it was assumed that the sample cooled stepwise to room temperature was oxygen-stoichiometric SnO_2. The right hand ordinate of Fig. 2 is therefore an oxygen content scale.

Fully reversible data were obtained over the range 700 – 1200 ^{o}C and are attributed to variation in oxygen content as a function of temperature in air. At lower temperatures, data were not reversible on the heat/cool cycle. An initial decrease in weight occurred at 200 ^{o}C which was attributable to loss of H_20 absorbed during the slow cool from 900 ^{o}C. The weight then increased again at 600 and 700 ^{o}C; this was attributed to uptake of O_2 by the sample that was still slightly oxygen-deficient, in spite of its slow cool in O_2 from 900 ^{o}C. Above 700 ^{o}C, the sample started to lose weight again and this continued to the highest temperature studied, 1200 ^{o}C.

From these experiments, it is concluded that :
(i) SnO_2 loses oxygen spontaneously and reversibly in air over the temperature range 700 to 1200 ^{o}C. At 1200 ^{o}C, for instance, its oxygen content is given by the formula $SnO_{1.9989(1)}$. Oxygen-deficient SnO_2 is expected to be an n-type semiconductor whose conductivity is sensitive to pO_2 and is given by the mechanism:

$$O_O^{x} \rightarrow \tfrac{1}{2} O_2 + 2e' + V_O^{\cdot\cdot} \qquad (1)$$

(ii) The rate of uptake of O_2 by oxygen-deficient $SnO_{2-\delta}$ during cooling is very temperature-dependent. Equilibrium is readily obtained down to 700 ^{o}C, but prolonged isothermal heating is required to achieve full, internal equilibrium at lower temperatures, although the gas-solid surface reactions proceed much more rapidly than those requiring diffusion into sample interiors. Several stages in the uptake and desorption of O_2 may be envisaged.

(iii) Oxygen-deficient $SnO_{2-\delta}$ is moisture-sensitive and, at lower temperatures, uptake of H_2O may take place more easily than uptake of O_2. It is presumed that H_2O uptake occurs by the reaction:

$$V_o^{\cdot\cdot} + 0_o^{x} + H_20 \rightarrow 2OH_o^{\cdot} \qquad (2)$$

(iv) The stoichiometry of both the surface and interior of SnO_2 pellets depends critically on the final cooling step, especially cooling rate and atmosphere. Thus, the overall level of oxygen deficiency, δ, may vary but in addition, concentration gradients in δ may exist, in which surfaces have smaller δ than grain interiors, especially if oxidation and equilibration are incomplete at a particular temperature. Similarly, gradients in concentration of adsorbed H_2O may be present on short exposure timescales. In order to assess the possible significance of these stoichiometry variations on electrical properties, IS measurements were made on pellets given a range of heat treatments.

Impedance data for a typical sample, with measurements at several temperatures, are shown in Fig 3. Data are presented in various ways to highlight different impedance characteristics of the sample and to allow a more comprehensive understanding of its electrical make-up and properties [22]. There are four widely-used impedance formalisms, the impedance, Z*, the admittance, Y*(or A*), the modulus, M* and the permittivity, (ε*). These are inter-related by:

$$Z^* = (Y^*)^{-1} = (j\omega C_o)^{-1}M^* = (j\omega C_o\varepsilon^*)^{-1} \qquad (3)$$

where ω is the angular frequency, 2πf and C_o is the vacuum capacitance of the sample. Data can be presented in any of the four formalisms, either as complex plane plots or as spectroscopic plots of one parameter against frequency. It is certainly not necessary to present data in all possible ways, but we find that the combination of plots used in Fig 3 usually permits a comprehensive overview of the electrical microstructure of a sample to be obtained.

Thus, for the data shown in Fig 3, complex plane plots, Z″ vs Z‘, (a), show a single, broad arc whose low frequency intercept on the Z‘ axis gives the total resistance of the sample, R_T. On replotting the same data as log Y‘ vs log f, (b), a low frequency plateau is seen with a conductivity value R_T^{-1} and a dispersion at high frequencies which moves off-scale with increasing temperature. These high frequency data show a power law dependence of log Y‘ on log f and are an example of Jonscher’s law of universal dielectric response[23] that is observed in many ionic and electronic conductors.

The same data replotted as log C′ vs log f, (c), show two plateaux with approximate values 3 and 20 pF whose interpretation is that the sample response contains both bulk (grain) and grain boundary impedances. Thus, a value of ~ 3 pF for the high frequency plateau corresponds to a permittivity of ~ 34 and is attributed to the sample bulk. The magnitude of the low frequency plateau is rather small for a conventional grain boundary of a well-sintered ceramic which suggests that it occupies a significant volume fraction of the sample. SEM data, Fig 1, show a porous microstructure of interconnected grains and the low frequency capacitance plateau is therefore attributed to a constriction resistance associated with the necks between adjacent grains together with the air gaps between grains[24]. Since the same material is usually present in the necks and grains, a characteristic feature of constriction resistances is that the activation energies of the grain and grain boundary resistances are similar.

A useful, pictorial overview of the electrical microstructure of the sample is obtained by replotting the same data as M″/Z″ vs log f (d); this type of presentation is also known as impedance and modulus spectroscopy[25]. A single peak is seen in the M″ spectrum which represents the smallest capacitance in the sample; this therefore, corresponds to the bulk impedance. The Z″ peak, scaled to be of similar height to the M″ peak for an easy visual assessment, occurs at similar, but slightly lower, frequency and additionally, contains a low frequency, poorly-resolved shoulder peak. The main Z″ peak therefore represents the bulk resistance as it overlaps with the M″ peak. The low frequency shoulder peak is the grain boundary resistance associated with the low frequency plateau seen more clearly in (c).

The small difference in peak maximum frequencies between the Z″ and M″ peaks is associated mainly with the constant phase element, CPE, in the equivalent circuit, Fig 4, that is used to model the impedance data. The admittance of the bulk element, R_1-C_1-CPE_1 in the circuit shown in Fig 4 is given by [26]:

$$Y^* = (R_1)^{-1} + j\omega C_1 + A_1\omega^n + jB_1\omega^n \quad (4)$$

where $(A_1/B_1) = \tan(n\pi/2)$ (5)

The CPE is, effectively, a parallel combination of a frequency-dependent resistor and capacitor; the relative contribution of each to the overall, frequency-dependent admittance is governed by the power law exponent, n[27].

The effect of including a CPE in the equivalent circuit may be seen by comparing the resulting impedance with that of an ideal parallel RC element, without a CPE, whose admittance is given by:

$$Y^* = (R)^{-1} + j\omega C \quad (6)$$

The resulting M″ and Z″ spectra of an ideal RC element consist of symmetric 'Debye peaks' with the functional form:

$$\text{Peak profile} = \frac{\omega RC}{1+(\omega RC)^2} \quad (7)$$

and for which the peak maxima are given by:

$$\omega RC = 1 \quad (8)$$

The peaks are scaled according to (C_0/C) for M″ and R for Z″ [22]. On introduction of a CPE in the equivalent circuit, characteristic changes are that (i) the M″ peak occurs at slightly higher frequency than the Z" peak, (ii) the M" peak is Debye-like on the low frequency side but broadened asymmetrically on the high frequency side and conversely, (iii) the Z" peak is broadened at low frequencies but Debye-like at high frequencies [26].

From the impedance data shown in Fig 3 and their interpretation in terms of the equivalent circuit shown in Fig 4, the electrical microstructure of the SnO_2 pellets appears to have the following characteristics:

(i) the total sample resistance is a combination of grain and grain boundary resistances connected in series.
(ii) the grain boundary impedance is the neck region connecting grains in the poorly-sintered, porous sample and is a constriction impedance.

The implication from this analysis is that the measured impedance represents that of the sample volume, not its surface. There was no evidence for the possible existence of a core-shell structure with conducting grains surrounded by resistive grain boundaries or surfaces. Thus, the high frequency capacitance data, Fig 3(c), show no evidence of a downturn to an additional plateau at still higher frequencies; similarly, the Y ' data show no evidence of an additional plateau of much higher conductivity at the highest frequencies. Both of these should have been apparent in the C', Y' data if the materials had conductive grain cores. In addition, the magnitude of the high frequency C' plateau is consistent with that expected for the bulk response of SnO_2. This interpretation is therefore used in the following analyses.

Total conductivity data were obtained either from the low frequency intercept on the Z' axis of the impedance complex plane plots, Fig 3(a) or from the low frequency Y' plateaux (b). Approximate values for the bulk conductivity were obtained from the M" spectra using equation 8 for the peak maximum frequency and equation 9 for the peak height:

$$M''_{max} = C_o/2C \qquad (9)$$

Bulk, σ_b and total, σ_T conductivity data for a range of samples are shown in Fig 5. Slow-cooled samples were measured in O_2 to avoid possible O_2 loss during the impedance measurements. By contrast, quenched samples were measured in N_2 to avoid possible oxidation during IS measurement. Conductivities were highest for samples quenched from the highest temperature, 1200 ^oC and lowest for samples slow-cooled in O_2; activation energies ranged from 0.52 to 1.10 eV. These data are fully consistent with n-type conduction that is controlled by the degree of oxygen nonstoichiometry, δ, Fig 2. Large changes in conductivity occur for very small changes in δ. Although the changes in δ are initiated by gas-solid reactions at sample surfaces, equation 1, the conductivities appear to be controlled by sample interiors rather than surfaces since both bulk and grain boundary components are detected in the impedance response, Fig 3. The bulk conductivities in Fig 5(a) are higher than the total conductivities, (b), and have slightly smaller activation energies. The higher activation energy of the total conductivity reflects the contribution of the grain boundaries to the total impedance, especially at lower temperatures: since the grain boundaries are generally more oxidised than the grains, they have smaller δ values and higher activation energies, as shown by the decrease in activation energy with increased reduction at higher quench temperature in Fig 5(a).

Changes in sample mass due to oxygen loss/gain were detected at temperatures as low as 600 ^oC, Fig 2; however, conductivity measurements in different atmospheres showed evidence of oxygen loss/gain at much lower temperatures, Fig 6. At eg 350 ^oC, the total conductivity of a sample slow-cooled in O_2 increased gradually by > 1 order of magnitude on changing the atmosphere to N_2. The initial conductivity was subsequently recovered by switching back to O_2; similar conductivity changes occurred more rapidly with increasing temperature. These conductivity changes, by 1-2 orders of magnitude, are less than the total range of conductivities, covering 4-5 orders of magnitude, that are obtainable at a particular temperature from variation in δ, Fig 5. The initial conductivity changes are clearly surface-controlled, therefore, whereas those that include exchange of species, such as oxygen vacancies, between sample interior and surface are important on longer time scales.

Conductivity data were also sensitive to moisture in the atmosphere, as shown in Fig 7 on changing the atmosphere between wet and dry N_2 at 300 ^oC for an oxygen-deficient sample prepared by quenching from 1000 ^oC. Conductivity increased by > 1 order of magnitude in wet N_2 with an associated reduction in activation energy. Sensitivity to moisture was, however, greatly dependent on sample history, as summarised in Fig 8 for quenched and slow-cooled samples measured in wet/dry N_2: the quenched sample was sensitive to moisture whereas the slow-cooled sample was not.

At present, we cannot comment on whether increased conductivity in a wet atmosphere is electronic or protonic. Proton conductivity certainly seems to be a possibility since proton conductivity at high temperature in doped cerate perovskite structures is well-established[28] and is attributed to proton transfer associated with OH groups that form on adsorption of H_2O by oxygen-deficient samples. However, there are comments in the literature concerning possible modification in the level of electronic conductivity and the band structure at the SnO_2 surface associated with water adsorption / desorption; further work is therefore required to determine the nature of the conducting species associated with H_2O adsorption.

It is important to understand the electronic and (possible) protonic contributions to the overall conductivity of a particular SnO_2 sample and how they vary depending on sample processing conditions and the atmosphere prior to and during, IS measurements. This is illustrated further by the changes seen on varying the atmosphere between dry and wet O_2, N_2 and CO_2 in Fig 9 at 400 ^oC. In O_2, the conductivity increased only slightly between dry and wet atmosphere. In dry N_2 or CO_2, the conductivity increased reversibly by 1-2 orders of magnitude and by an additional 1-2 orders of magnitude on switching to wet atmospheres. The first increase, in dry atmospheres, can be attributed to increased electronic conduction associated with loss of O_2 on reducing pO_2 in the surrounding atmosphere. The second increase, on changing to a wet atmosphere, may be due to proton conduction or alternatively, to electronic conduction if the SnO_2 band structure changes on H_2O uptake.

These results obtained in dry atmospheres show that conductivity changes seen in CO_2 are attributable directly to changes in δ since similar results are seen in both N_2 and CO_2. SnO_2 is therefore only an *indirect* sensor of CO_2, as the sensing mechanism involves exchange of O_2 between the sample and the surrounding atmosphere and not direct interaction between CO_2 and SnO_2. Furthermore, these results show the importance of oxygen vacancies in order for H_2O adsorption to occur, but also, that oxygen vacancies can be created during the conductivity measurements. Thus, in a

moist N_2 atmosphere, desorption of O_2 may occur, allowing subsequent absorption of H_2O by the mechanism shown in equation (2).

The changes in electronic conductivity associated with adsorption/desorption of O_2 are represented simplistically by equation (1) but in reality, a much more complex sequence of processes is likely to occur, involving a series of equilibria that can be displaced in either direction, depending on pO_2, as follows:

$$O_2(g) \overset{1}{\leftrightarrow} O_2\,(ads) \overset{2,e}{\leftrightarrow} O_2^- \overset{3,e}{\leftrightarrow} O_2^{2-} / O^- \overset{4,e}{\leftrightarrow} O^{2-}\,(s) \overset{5}{\leftrightarrow} O^{2-}\,(bulk) \qquad (10)$$

where *g, ads* and *s* refer to gas phase, adsorbed species and surface. Equilibria 1 and 5 do not involve electron transfer, but any of equilibria 2, 3 and 4 should be detected by IS since, although the equilibria involve reactions at the gas-solid interface, electrons are likely to be withdrawn from/added to the sample interior as part of the redox reactions. Evidence for the different oxygen species at sample surfaces, which are involved in the equilibria shown in (10), was obtained from TPD studies [14] which showed that increasingly higher temperatures were required to release species adsorbed as O_2 (g), O_2^-, O^-/O^{2-} and O^{2-} (bulk). This is entirely consistent with our conclusion that step 5, leading to full equilibration of oxygen stoichiometry and distribution throughout the sample bulk, requires temperatures above 600-700 ^oC for it to be achieved on reasonable timescales.

Although changes to the equilibria 2, 3 and 4 would be detected by IS, an additional possibility that would probably not be detected by IS involves electron transfer between underbonded lattice 0^{2-} ions and adsorbed oxygen molecules, as in:

$$O^{2-} + O_2\,(\text{ads}) \leftrightarrow O^- + O_2^- \qquad (11)$$

The resulting O^- ions may then act as sources of hole conduction. Hole conductivity associated with the location of holes on oxygen as O^- ions in acceptor-doped titanate perovskites[29], Ca-doped $BiFe0_3$ [30] and yttria-stabilised zirconia[31] has been attributed to electron transfer processes involving underbonded oxide ions. Hence, the equilibria shown in (11) provide a modification to step 2 in (10), by assigning the source of electrons involved in the redox process to underbonded O^{2-} ions rather than to those associated with the n-type conduction mechanism. Reactions such as (11) could occur at SnO_2 surfaces and involve underbonded oxide ions that are not surrounded by a full complement of positive (cation) charge and indeed, evidence for species such as O^- and O_2^- is widely cited in surface science studies [32].

The literature contains very many reports on SnO_2 gas sensors, the variety of atomic and molecular steps that occur at sensor surfaces, the effect of sensor

microstructure and the nature of sample – electrode contacts, all of which have been reviewed [3, 32]. *ac* impedance measurements have also been used on numerous occasions [33-35] and resistivity changes associated with change in oxygen pressure have been reported [36, 37]. The novelty of the present work concerns impedance measurements as a function of temperature and atmosphere on carefully-prepared samples with different oxygen contents. From our results, it appears that the conductivity that is measured is a combination of grain and grain boundary conductivities associated with the sample bulk, even though sensing action involves gas-solid interactions at sample surfaces.

Models for sensing action that are discussed in the literature frequently are based on the creation of Schottky barriers and depletion layers. We find no evidence for Schottky barriers since our impedance data can be satisfactorily interpreted in terms of low-capacitance bulk and grain boundary impedances: Schottky barriers at sample-electrode interfaces would lead to additional thin layer impedances with associated capacitances typically in the nanoFarad range, in contrast to the picoFarad range of capacitances observed here. It would, however, be useful to confirm this conclusion by I-V measurements.

The concept of depletion layers may usefully be applied in our case since O_2 absorption at sample surfaces is associated with electron withdrawal from sample interiors, leading to positively-charged depletion layers. However, we see no evidence in the impedance data for conducting grain cores surrounded by more resistive depletion layers; the implication of this is that the depletion layer thickness is greater than the sizes of the grains.

CONCLUSIONS

SnO_2 pellets show a small, reversible loss of oxygen, in air, at temperatures above about 600 ^oC. Samples also lose oxygen reversibly at lower temperatures, eg 350 ^oC, simply by switching the atmosphere between O_2 and N_2, but the changes are confined to sample surfaces, at least on short timescales. The weight changes, which are detectable using a microbalance and a 2 g pellet, cause a change in *n*-type conductivity by several orders of magnitude, depending on the level of oxygen nonstoichiometry, δ.

Sample conductivity, and its sensitivity to gases, depends critically on the sample history. Thus, quenched, oxygen-deficient samples are sensitive to moisture uptake whereas slow-cooled, oxygen-stoichiometric samples are not. CO_2 and N_2 show a similar sensor response, attributable to desorption of O_2 in both cases.

Impedance spectroscopy provides evidence for grain and grain boundary contributions to the overall sample impedance, both of which show a similar sensor response. Although the sensor response involves gas – solid surface reactions, it appears that the measured conductivity changes are bulk conductivities and not surface conductivities.

ACKNOWLEDGEMENTS

IAA thanks the Libyan Embassy for financial support

REFERENCES

1. D.E. Williams in 'Solid State Gas Sensing' ed. P.T. Moseley and B.C. Tofield, Adam Hilger, Bristol (1987)
2. V.E. Henrich and P.A. Cox, 'The surface science of metal oxides', Cambridge University, Press (1994)
3. M. Batzill and U. Diebold, Progr. Surf. Sci., **79** (2005) 47
4. H-C. Shin, J. Dong and M. Liu, Adv. Mater., **16** (2004) 237
5. F. Morazzoni *et al*, Mater. Sci. Eng., **C15** (2001) 167
6. A. Forleo *et al*, Procedia Chemistry, **1** (2009) 196
7. E.Y. Sevastyanov *et al*, Semiconductors, **46** (2012) 801
8. Y.Z. Zhang *et al*, Int. J. Electrochem. Sci., **8** (2013) 3371
9. A. Yamaguchi *et al*, Thin Solid Films, **519** (2011) 2415
10. J. Pan *et al*, Chem. Commun., **50** (2014) 7020
11. S. Hwang *et al*, J. Amer. Ceram. Soc., **95** (2012) 324
12. R. Savu *et al*, Mater. Res., **12** (2009) 83
13. M. Batzill, W. Bergermayer, I. Tanaka and U. Diebold, Surf. Sci., **600** (2006) L29
14. N. Yamazoe, J. Fuchigami, M. Kishikawa and T. Seiyama, Surf. Sci., **86** (1979) 335
15. N. Barsan and R. Ionescu, Sensors and Actuators **B12** (1993) 71
16. V.A. Gercher and D.F. Cox, Surf. Sci., **322** (1995) 177
17. G. Korotchenkov, V. Brynzari and S. Dmitriev, Sensors and Actuators, **B54** (1999) 197.
18.T.F. McAleer, P.T. Moseley, J.O.W. Norris and D. E. Williams, Faraday Trans., **83** (1987) 1323.
19. J. Tamaki *et al*, Surf. Sci., **221** (1989) 183.
20. K. Watanabe et al, IMCS 2012 – The 14th Int. meeting on chemical sensors, DOI 10.5162/IMCS 2012/P.2.0.9, 1285.
21. Y. Liu and A. R. West, J Amer. Ceram. Soc., **96** (2013) 218.
22. J.T.S. Irvine, D.C. Sinclair and A.R. West, Adv. Mater., **2** (1990) 132
23. A.K. Jonscher, Dielectric relaxation in solids, Chelsea Dielectrics Press, London, (1983)

24. P.G. Bruce and A.R. West, J. Electrochem. Soc., **130** (1983) 662
25. I.M. Hodge, M.D. Ingram and A.R. West, J. Electroanal. Chem., **74** (1976) 125
26. D.P. Almond and A.R. West, J. Electroanal. Chem., **186** (1985) 17
27. D.P. Almond, C.R. Bowen and D.A.S. Rees, J. Phys. D, Appl. Phys., **39** (2006) 1295
28. H. Uchida *et al*, Solid State Ionics, **36** (1989) 89
29. H. Beltran *et al*, J. Amer. Ceram. Soc., **94** (2011) 2951
30. N. Maso *et al*, Phys. Chem. Chem. Phys., **16** (2014) 19408
31. N. Maso and A.R. West, Chem. Mater., **27** (2015) 1552
32. W. Gopel and K.D. Schierbaum, Sensors and Actuators, **B26-27** (1995) 12
33. G. Martinelli *et al*, Sensors and Actuators, **B26-27** (1995) 53
34. M. Labeau *et al*, Sensors and Actuators, **B26-27** (1995) 49
35. U. Weimar and W. Gopel, Sensors and Actuators **B26-27** (1995) 13
36. G. Blaustein *et al*, Sensors and Actuators **B55** (1999) 33
37. F. Schipani *et al,* J. Appl. Phys., **116** (2014) 194502

FIGURE CAPTIONS

1. Microstructure of a typical sintered pellet of SnO_2
2. Change in mass and oxygen content of SnO_2 as a function of temperature; red crosses: stepwise heating of a sample slow-cooled from 900 ^oC; yellow squares: stepwise cooling from 1200 ^oC. The errors in the mass measurements, +/- 0.00002 g, are within the size of the data points.
3. A typical impedance data set collected at 5 temperatures
4. Equivalent circuit used to analyse impedance data
5. (a)bulk and (b)total conductivities of SnO_2 pellets given different heat treatments after initial sintering at 1300 ^oC. All samples were quenched from the temperatures stated apart from 900 SC which was slow-cooled in oxygen from 900 ^oC
6. Effect of pO_2 in a dry atmosphere on the total conductivity of an SnO_2 pellet prepared by slow cooling from 1000 ^oC and then held in O_2 for 1 hour before IS measurements
7. Effect of a dry / wet atmosphere on the conductivity, in N_2, of an SnO_2 pellet quenched from 1000 ^oC; data recorded at 300 ^oC
8. Effect of atmosphere, moisture and sample history on conductivity of SnO_2 pellets. SC: slow cool; Q: quenched from 1000 ^oC
9. Time-dependent response of the total conductivity of a slow-cooled SnO_2 pellet at 400 ^oC to a range of dry and wet atmospheres

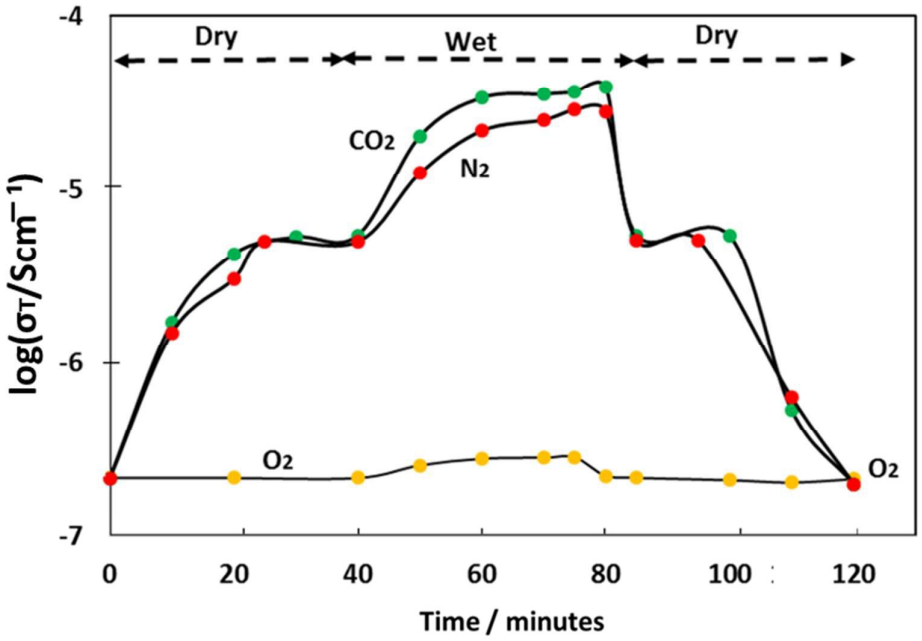

Sensitivity of SnO2 to different dry and wet gases